

On the radial abundance gradients in disks of irregular galaxies

L.S. Pilyugin^{1,2,3}, E.K. Grebel¹, I.A. Zinchenko^{1,2}

¹ *Astronomisches Rechen-Institut, Zentrum für Astronomie der Universität Heidelberg, Mönchhofstr. 12–14, 69120 Heidelberg, Germany*

² *Main Astronomical Observatory of National Academy of Sciences of Ukraine, 27 Zabolotnoho str., 03680 Kiev, Ukraine*

³ *Kazan Federal University, 18 Kremlyovskaya St., 420008, Kazan. Russian Federation*

Accepted 2015 April 22. Received 2015 April 22; in original form 2015 January 01

ABSTRACT

We determine the radial abundance distributions across the disks of fourteen irregular galaxies of the types *Sm* and *Im* (morphological *T* types $T = 9$ and $T = 10$) as traced by their H II regions. The oxygen and nitrogen abundances in H II regions are estimated through the T_e method or/and with the counterpart method (*C* method). Moreover, we examine the correspondence between the radial abundance gradient and the surface brightness profile. We find that irregular galaxies with a flat inner profile (flat or outwardly increasing surface brightness in the central region) show shallow (if any) radial abundance gradients. On the other hand, irregular galaxies with a steep inner profile (with or without a bulge or central star cluster) usually show rather steep radial abundance gradients. This is in contrast to the widely held belief that irregular galaxies do not usually show a radial abundance gradient.

Key words: galaxies: irregular – galaxies: abundances – ISM: abundances – H II regions – galaxies: photometry

1 INTRODUCTION

The radial distribution of gas-phase oxygen abundances traced by H II regions has been investigated in the disks of many spiral galaxies (Vila-Costas & Edmunds 1992; Zaritsky et al. 1994; van Zee et al. 1998; Pilyugin et al. 2004; Moustakas et al. 2010; Gusev et al. 2012; Pilyugin et al. 2014a; Sánchez et al. 2014). It was found that almost all spiral galaxies show radial abundance gradients in the sense that their inner H II regions (i.e., those closer to the galactic centers) have higher oxygen abundances than the outer ones.

The radial distribution of abundances across the disks of irregular galaxies is less well studied. Pagel et al. (1978) analyzed spectra of a number of H II regions in the Small and Large Magellanic Clouds. They determined the abundances in H II regions through the effective temperature (T_e) method using their own measurements together with the spectral measurements by other authors and examined the spatial distributions of abundances in those galaxies. Pagel et al. (1978) concluded that any radial abundance gradient in present-day abundances is small or absent in the Large Magellanic Cloud and is conspicuously absent in the Small Magellanic Cloud. In the Small Magellanic Cloud, also stellar metallicity determinations support the absence of a radial gradient, although there is a large metallicity spread of ~ 0.6 dex in $[\text{Fe}/\text{H}]$ for a given age (Glatt et al. 2008; Cignoni et al. 2013).

Roy et al. (1996) studied the oxygen abundance distributions in the disks of the dwarf irregular galaxy NGC 2366 and the dwarf Seyfert I galaxy NGC 4395 using imaging spectrophotometry with narrow-band filters in the lines of $\text{H}\alpha$, $\text{H}\beta$, $[\text{O III}]\lambda 5007$ and $[\text{N II}]\lambda 6584$. They used the line ratio $[\text{O III}]/[\text{N II}]$ as an abundance

indicator (O3N2 calibration). They found that there is no global oxygen abundance gradient across the disks of those galaxies.

Hunter & Hoffman (1999) obtained emission-line long-slit spectra of 189 H II regions in a sample of 65 *Im*, *Sm*, and blue compact dwarf galaxies. They estimated the oxygen abundances in H II regions using the line ratio $[\text{O III}]/[\text{N II}]$ (O3N2 calibration) and the combination of $R_{23} = [\text{O III}] + [\text{O II}]$ and $[\text{O III}]/[\text{O II}]$ (two-dimensional R_{23} calibration) when the oxygen line $[\text{O II}]\lambda 3727$ was measured. Hunter & Hoffman (1999) examined the radial abundance distribution in disks of eight *Sm* and *Im* galaxies for which they measured at least three H II regions. They found that the oxygen abundances within a given galaxy generally vary by about 0.2 dex, but they did not detect a trend in oxygen abundances with radius except for the *Sm* galaxy DDO 204.

Kniazev et al. (2005) measured oxygen abundances with the direct method in three H II regions in each of the dwarf irregulars Sextans A and Sextans B. While they found Sex A to be chemically homogeneous, one of the three H II regions in Sex B turned out to be about twice as metal-rich than the other two, and the abundances of other heavy elements suggest an enrichment by a factor of ~ 2.5 as compared to the other two H II regions. Kniazev et al. (2005) attribute this to inhomogeneous chemical enrichment.

van Zee & Haynes (2006) carried out long-slit spectroscopy of 67 H II regions in 21 dwarf irregular galaxies. Oxygen abundances for 25 H II regions were derived through the direct T_e method; the abundances in other H II regions were estimated using strong line calibrations. van Zee & Haynes (2006) considered the oxygen abundances as a function of radius for 12 irregular galaxies with three or more observations and found that the abundances are very similar (within the formal errors) within each galaxy with the

arXiv:1505.00337v1 [astro-ph.GA] 2 May 2015

possible exception of the galaxy UGC 12894. van Zee & Haynes (2006) noted that the radial trend in oxygen abundances (three points) in the UGC 12894 may be artificial because the abundances of the inner and outer H II regions were obtained via different methods (through the strong line calibration for two inner H II regions and through the T_e method for outer H II region).

Similarly, Lee et al. (2007) obtained oxygen abundances for 35 H II regions in eight dwarf galaxies in the Centaurus A group and in 13 H II regions in closer dwarfs. Some of their measurements use the direct T_e method, while the majority of the abundance determinations is based on strong-line calibrations. Although the results for individual H II regions in a given galaxy tend to vary, Lee et al. point out that the variations are within the uncertainties of the strong-line method. In one of the dwarf irregulars of the Cen A group, AM 1318–444, one of the H II regions is considerably more oxygen-rich than the others. Lee et al. argue that the measured line intensity ratios suggest that this emission nebula is a supernova remnant. They also note that radial gradients may exist in some of their targets such as in the *Sm* NGC 3109 or NGC 5264, but that more and deeper data are needed to establish this.

It is the current belief that irregular galaxies generally do not show radial abundance gradients in their young populations and are chemically homogeneous. This implies that there is a “spiral versus irregular dichotomy” in the sense that there is a sudden change from spiral (radial abundance gradients are usually present) to irregular galaxies (typically no gradients). However, other properties (e.g., gas fraction, global metallicity) vary smoothly in transition from spirals to irregulars (Zaritsky et al. 1994; Pilyugin & Ferrini 2000; Garnett 2002; Pilyugin et al. 2007, among others).

The measurements of the abundance gradients in the disks of irregular galaxies often encounter the following difficulty. Reliable oxygen abundances in a number of H II regions in the disk of a galaxy should be determined in order to evaluate the existence of an abundance gradient. Abundance determinations using the direct T_e method require high-precision spectroscopy including the weak auroral lines [O III] λ 4363 or/and [N II] λ 5755. Unfortunately, these weak auroral lines are usually only detected in the spectra of a few (if any) of the brightest H II regions in a given irregular galaxy. The oxygen abundances in the other H II regions are then estimated using the strong-line method pioneered by Pagel et al. (1979) and Alloin et al. (1979). The principal idea of the strong-line method is to establish the relation between the (oxygen) abundance in an H II region and some combination of the intensities of strong emission lines in its spectrum (such a relation is usually called a “calibration”). Different calibrations were suggested. A prominent characteristic of the calibrations is that they are not applicable across the whole range of metallicities of H II regions but only within a limited interval (usually only at high or at low metallicities). The oxygen abundances of irregular galaxies typically lie within or near the transition zone in the $R_{23} - \text{O}/\text{H}$ diagram (from $12 + \log(\text{O}/\text{H}) \sim 7.9$ to ~ 8.3) where calibrations cannot be used or where they provide abundances with large uncertainties.

We recently suggested a new method (the “C method”) for abundance determinations in H II regions, which can be used over the whole range of metallicities of H II regions and which provides oxygen and nitrogen abundances on the same metallicity scale as the classic T_e method (Pilyugin et al. 2012, 2013). Using this method, we examined the abundance gradients in the disks of 130 late-type galaxies including several irregular galaxies (Pilyugin et al. 2014a). In that study, radial abundance gradients were found in irregular galaxies. Here we will focus on the investigation of the abundance gradients in a sample of irregular

galaxies (*Sm* and *Im*, morphological T types 9 and 10). Since there is a relation between oxygen abundance and disk surface brightness in spiral galaxies (e.g., Pilyugin et al. 2014b), we will also examine the relation between radial abundance distributions and surface brightness profiles of the disks of irregular galaxies.

The paper is structured as follows. The spectral and photometric data are reported in Section 2. The radial abundance gradients are determined in Section 3. The discussion and conclusions are given in Section 4, followed by a summary (Section 5).

2 THE DATA

2.1 Our sample

We have selected a sample of irregular *Sm* and *Im* and galaxies with morphological T types of 9 and 10 according to the RC3 catalog (de Vaucouleurs et al. 1991). It should be noted that the morphological classification of some galaxies is not robust. The morphological T types in different sources can differ by up to 1. We only consider irregular galaxies with available spectra for four and more H II regions. The validity of the radial abundance is defined not only by the quantity and quality of the spectra but also by the distribution of the measured H II regions along the galactic radius. We reject galaxies where the measured H II regions cover less than $\sim 1/3$ of the optical radius of a galaxy. For example, for this reason we rejected the galaxy UGC 5666 (a.k.a. IC 2574 or DDO 81). More than ten spectra are available for this galaxy (Miller & Hodge 1996; Croxall et al. 2009), but the measured H II regions cover only a small fraction of the optical radius of the galaxy, which prevents a reliable investigation of a radial abundance gradient.

Our final list includes fourteen irregular galaxies with optical radii of $R_{25} \geq 2$ kpc. Table 1 lists the general characteristics of each galaxy. The column 1 contains the order number. The columns 2 – 4 give the galaxy’s name. We list the number of a galaxy according to the New General Catalogue (NGC, column 2), the Uppsala General Catalog of Galaxies (UGC, column 3), and one other widely used name (column 4). The morphological type of the galaxy (morphological type code T) from the RC3 is reported in column 5. The right ascension (R.A.) and declination (Dec.) (J2000.0) of each galaxy are given in columns 6 and 7. The right ascension and declination are obtained from our photometry (see Section 2.3) or taken from the NASA/IPAC Extragalactic Database (NED)¹. The position angle (P.A.), axis ratio (b/a), and inclination are listed in columns 8 – 10. The isophotal radius R_{25} in arcmin and in kpc of each galaxy is reported in columns 11 and 12, respectively. The adopted distance d taken from Karachentsev et al. (2013) or from the NED is reported in column 13. The NED distances use flow corrections for Virgo, the Great Attractor, and Shapley Supercluster infall. The references to sources for geometrical parameters (first reference) and for distances (second reference) are given in column 14.

2.2 Emission line intensities in the H II region spectra

We use the emission line intensities in published spectra of H II regions from different works for abundance determinations. We have searched for spectra of H II regions with measured H α , H β ,

¹ The NASA/IPAC Extragalactic Database (NED) is operated by the Jet Propulsion Laboratory, California Institute of Technology, under contract with the National Aeronautics and Space Administration. <http://ned.ipac.caltech.edu/>

Table 1. The adopted properties of our galaxies.

n	Name		T	R.A.	Dec.	P.A.	b/a	Inclination	R_{25}	R_{25}	d	Reference
	NGC	UGC	Other	type				degree	arcmin	kpc	Mpc	
1		2023	DDO 25	10	02:33:18.20	33:29:28.0	1.00	0	0.83	2.24	9.30	RC3; K13 ^a
2		2216		10	02:44:21.14	00:40:37.6	0.41	66	0.40	4.25	36.50	Here; NED
3	1156	2455		10	02:59:42.30	25:14:16.2	0.74	42	1.66	3.76	7.80	RC3; K13
4	2537	4274		9	08:13:14.66	45:59:32.7	0.95	18	1.07	3.80	12.20	Here; K13
5		4305	DDO 50	10	08:19:04.98	70:43:12.1	0.79	37	3.97	3.92	3.39	RC3; K13
6	3738	6565		10	11:35:48.81	54:31:25.8	0.66	49	1.43	2.04	4.90	Here; K13
7		6980		10	11:59:06.20	24:28:20.3	0.48	61	0.23	3.55	53.10	Here; NED
8	4214	7278	NGC 4228	10	12:15:39.19	36:19:36.6	0.89	27	3.18	2.72	2.94	Here; K13
9	4395	7524		9	12:25:48.88	33:32:48.7	0.64	50	4.08	5.47	4.61	Here; K13
10		7557		9	12:27:11.24	07:15:47.1	0.80	37	1.14	4.54	13.70	Here; NED
11	4449	7592		10	12:28:11.01	44:05:38.1	0.56	56	3.07	3.76	4.21	Here; K13
12			CGCG 071-090	10	12:58:52.80	13:09:08.8	0.60	53	0.49	1.98	13.90	Here; NED
13		9614		10	14:56:47.70	09:30:33.4	0.77	40	0.50	7.23	49.70	Here; NED
14		12709	DDO 219	9	23:37:24.05	00:23:30.7	0.73	43	0.73	7.86	37.00	Here; NED

^a K13 – Karachentsev et al. (2013)

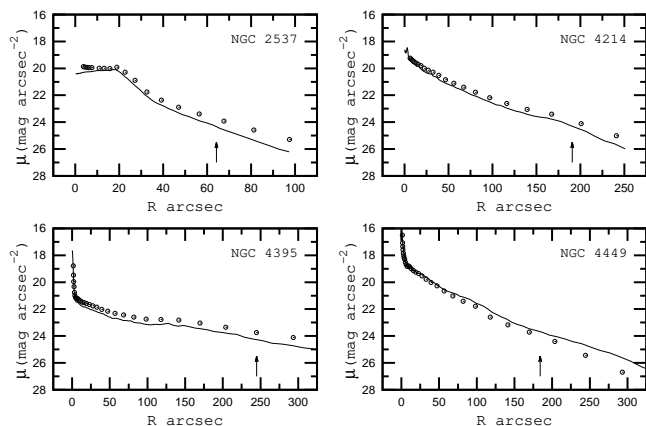


Figure 1. Comparison between the measured surface brightness profiles in the SDSS r band (line) obtained here and profiles in the R band (open circles) from Swaters & Balcells (2002). The arrow marks the optical isophotal radius R_{25} .

[O III] λ 5007, [N II] λ 6584, and [S II] λ 6717+ λ 6731 lines. The lines [O II] λ 3727+ λ 3729 and [O III] λ 4363 are also available in a number of spectra. We have taken the de-reddened line intensities as reported by the authors. If only the measured fluxes are given then the measured emission-line fluxes were corrected for interstellar reddening in the same way as in Pilyugin et al. (2014a). These spectroscopic data form the basis for the abundance determinations. The references to the spectroscopic data sources are listed in Table 2.

2.3 Surface brightness profiles

We constructed radial surface brightness profiles in the infrared $W1$ band (with an isophotal wavelength of $3.4 \mu\text{m}$) using the publicly available photometric maps obtained in the framework of the *Wide-field Infrared Survey Explorer* (*WISE*) project (Wright et al. 2010). The conversion of the photometric map into the surface brightness profile is discussed in Pilyugin et al. (2014b). Parameters such as the galaxy center, the position angle of the major axis, and the axis ratio are obtained through fitting of the isophotes by ellipses.

We also constructed radial surface brightness profiles in the

SDSS g and r bands using the photometric maps of SDSS data release 9 (Ahn et al. 2012). To estimate the optical isophotal radius R_{25} of a galaxy, the surface brightnesses in the SDSS filters g and r were converted to B -band brightnesses, and the AB magnitudes were reduced to the Vega photometric system using the conversion relations and solar magnitudes of Blanton & Roweis (2007).

Swaters & Balcells (2002) reported surface brightness profiles in the R band for a large number of galaxies. Fig. 1 shows the comparison between our measured surface brightness profiles in the SDSS r band (solid line) and R -band profiles (open circles) from Swaters & Balcells (2002). Our surface brightness profiles within the optical isophotal radius R_{25} agree satisfactorily well with those of Swaters & Balcells (2002).

All surface brightness measurements were corrected for Galactic foreground extinction using the A_V values from the recalibration of the maps of Schlegel et al. (1998) by Schlafly & Finkbeiner (2011) and the extinction curve of Cardelli et al. (1989), assuming a ratio of total to selective extinction of $R_V = A_V/E_{B-V} = 3.1$. The A_V values given in the NASA Extragalactic Database (NED) were adopted. To transform the surface brightness measurements to solar units, we used the magnitude of the Sun in the $W1$ band, which we obtained from its magnitude in the V band and from its color $(V - W1)_\odot = 1.608$ taken from Casagrande et al. (2012).

The radial profiles in the SDSS g and r bands were used to estimate the isophotal R_{25} radius of each galaxy. The obtained radial profiles were reduced to a face-on galaxy orientation. Note that the inclination correction is purely geometrical, and it does not include any correction for inclination-dependent internal obscuration. The values of the optical radius R_{25} determined here are listed in Table 1. There are no SDSS photometric maps for several galaxies of our sample. The optical radii R_{25} (as well as the position angle of the major axis and the inclination angle) for those galaxies were taken from the RC3 (de Vaucouleurs et al. 1991).

The observed surface brightness profile of an irregular galaxy can be fitted by an exponential (Swaters & Balcells 2002; Herrmann et al. 2013). There are bulges, bars, or nuclear star clusters at the centres of some irregular galaxies. A bulge or a nuclear star cluster can be fitted with a general Sérsic profile. A profile showing an increase of (optical) surface brightness in the central part

of a galaxy (with or without bulge-like component) will be referred to as a steep inner profile below. Irregular galaxies with a steep inner profile are presented in Fig. 2.

It is known that the surface brightnesses in some irregular galaxies are flat or even increase out to a region of slope change where they tend to fall off (Swaters & Balcells 2002; Taylor et al. 2005; Herrmann et al. 2013). Such surface brightness profiles can be formally fitted by an exponential disk with a bulge-like component of negative brightness. Such profiles will be referred to as flat inner profiles below. Irregular galaxies with flat inner profiles are presented in Fig. 3.

To define the type of surface brightness profile we use our surface brightness profiles in the SDSS *r* band or *R*-band profiles from Swaters & Balcells (2002). It should be noted that the shapes of the surface brightness profiles of the same galaxy in the different photometric bands do not necessarily coincide with each other.

3 ABUNDANCES

3.1 Abundance determination

We determine the T_e -based oxygen $(\text{O}/\text{H})_{T_e}$ and nitrogen $(\text{N}/\text{H})_{T_e}$ abundances in H II regions where the auroral line $[\text{O III}]\lambda 4363$ is detected using the equations of the T_e -method from Pilyugin et al. (2010, 2012).

A new method (called the ‘‘C method’’) for oxygen and nitrogen abundance determinations from strong emission lines has recently been suggested (Pilyugin et al. 2012, 2013). Here, the strong lines $R_3 = [\text{O III}]\lambda\lambda 4959, 5007$, $N_2 = [\text{N II}]\lambda\lambda 6548, 6584$ and $S_2 = [\text{S II}]\lambda\lambda 6717, 6731$ are used in the determinations of the oxygen $(\text{O}/\text{H})_{C_{NS}}$ and nitrogen $(\text{N}/\text{H})_{C_{NS}}$ abundances in individual H II regions of our target galaxies.

3.2 Radial abundance gradients

The deprojected radii of the H II regions were computed using their coordinates and geometrical parameters (position angle of the major axis and galaxy inclination) listed in Table 1.

The radial oxygen abundance distribution within the isophotal radius in every galaxy was fitted by the following equation:

$$12 + \log(\text{O}/\text{H}) = 12 + \log(\text{O}/\text{H})_{R_0} + C_{O/H} \times (R/R_{25}), \quad (1)$$

where $12 + \log(\text{O}/\text{H})_{R_0}$ is the oxygen abundance at $R_0 = 0$, i.e., the extrapolated central oxygen abundance. $C_{O/H}$ is the slope of the oxygen abundance gradient expressed in terms of dex R_{25}^{-1} , and R/R_{25} is the fractional radius (the galactocentric distance normalized to the disk’s isophotal radius R_{25}). The derived parameters of the oxygen abundance distributions are presented in Table 2. The name of the galaxy is listed in column 1. The optical isophotal radius R_{25} in kpc is reported in column 2. The extrapolated central $12 + \log(\text{O}/\text{H})_{R_0}$ oxygen abundance and the gradient expressed in terms of dex R_{25}^{-1} are listed in columns 3 and 4 (the bootstrapped error of the gradient is given in parenthesis). The scatter of oxygen abundances around the general radial oxygen abundance trend is reported in column 5. The references to sources for spectroscopic data are given in column 9. The radial distributions of the oxygen abundances in irregular galaxies are shown in Figs. 2 and 3 together with the surface brightness profiles.

The statistical error of the gradient listed in column 4 comes from the best fitting procedure. We also estimate the bootstrapped

error of the gradient in the following way. The measured H II regions in a galaxy are numbered from 1 to n . We then produce n random integer numbers using a random number generator, and form a bootstrapped subsample of H II regions choosing the corresponding H II regions from the original sample of H II regions. The amount of H II regions in the bootstrapped subsample is adopted to be equal to the amount of the H II regions in the original sample. Thus, some H II regions from the original sample can be repeatedly included in the bootstrapped subsample while other H II regions from the original sample will not at all be included in the bootstrapped subsample. If a bootstrapped subsample involves less than three different H II regions then this subsample is rejected. The abundance gradient for the bootstrapped subsample is determined through the best fit, and the error of the original gradient, i.e., the difference between the values of the gradients for the bootstrapped subsample and for the original sample of H II regions is obtained. We considered $k = 10^5$ bootstrapped subsamples and determined the bootstrapped error of the gradient as $([(\sum \text{difference}_j^2)/k]^{1/2})$. This bootstrapped error of the oxygen abundance gradient is given in Table 2, column 4 in parenthesis.

The statistical and bootstrapped errors of the oxygen abundance gradients are close to each other except in the case of the galaxy UGC 2216 where the bootstrapped error exceeds dramatically the statistical error. This is caused by the following. The radial abundance gradient in the UGC 2216 is strongly biased by an H II region at a galactocentric distance of 4.43 kpc. When the bootstrapped subsample does not contain this point then the value of the radial abundance gradient is very uncertain since in this case the gradient is determined from measurements at close galactocentric distances. As a result, the bootstrapped error of the radial abundance gradient for this galaxy is quite large.

As in the case of the oxygen abundance, the radial nitrogen abundance distribution in every galaxy was fitted by the following equation:

$$12 + \log(\text{N}/\text{H}) = 12 + \log(\text{N}/\text{H})_{R_0} + C_{N/H} \times (R/R_{25}). \quad (2)$$

The derived parameters of the nitrogen abundance distributions are presented in Table 2. The extrapolated central $12 + \log(\text{N}/\text{H})_{R_0}$ nitrogen abundance and the gradient in terms of dex R_{25}^{-1} are listed in columns 6 and 7. The scatter of oxygen abundances around the general radial oxygen abundance trend is reported in column 8. The value in the parenthesis in column 7 is the bootstrapped error of the nitrogen abundance gradient obtained in the same way as for the oxygen abundance gradient.

The radial oxygen abundance gradients in irregular galaxies obtained here are based mainly (or only) on oxygen abundances $(\text{O}/\text{H})_{C_{NS}}$ estimated through strong emission lines using the C_{NS} method. Figs. 2 and 3 show that the scatter in the $(\text{O}/\text{H})_{C_{NS}}$ abundances around the general radial trend is often lower than the scatter in the $(\text{O}/\text{H})_{T_e}$ abundances. Five galaxies from our present sample are in the list of galaxies considered in our previous study (Pilyugin et al. 2014a). The values of gradients obtained here are slightly different from those reported in our previous study for the following reasons. First, in our current work we obtain and use new parameters for our target galaxies such as inclination, position angle of the major axis, and optical isophotal radius. Furthermore, in Pilyugin et al. (2014a) the oxygen and nitrogen abundances were estimated via the C_{ON} method for H II regions with available measurements of the $[\text{O II}]\lambda\lambda 3727, 3729$ emission line, and with the C_{NS} method for the other H II regions. In our current study, the oxygen and nitrogen abundances were estimated through the C_{NS} method for all H II regions, and T_e -based abundances are added.

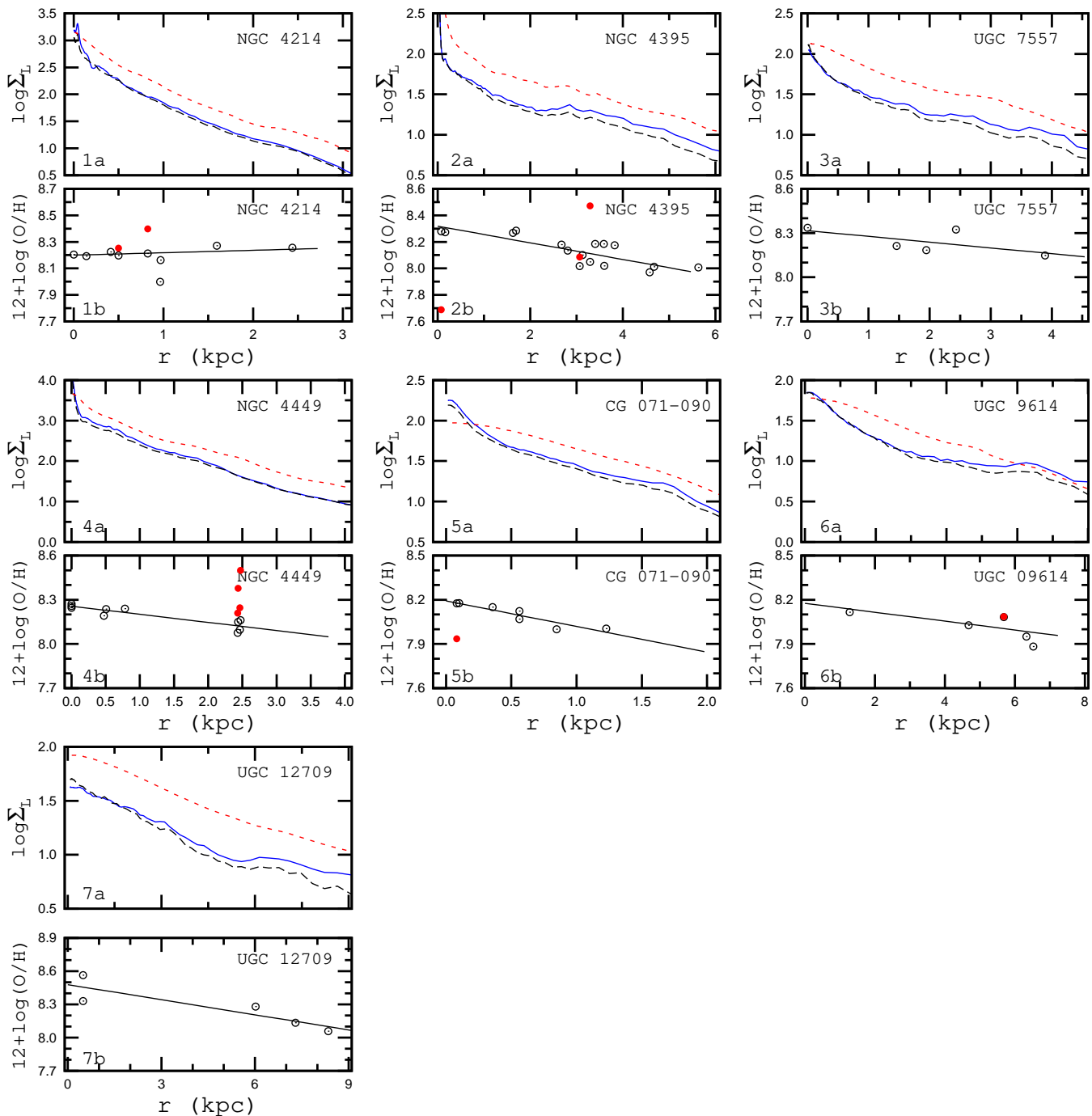


Figure 2. Surface brightness profiles and radial distributions of oxygen abundances for irregular galaxies with steep inner profiles. Each galaxy is presented in two panels. Each upper panel *Na* shows the surface brightness profiles in the SDSS *g* band as a light-grey (blue) solid line, in the SDSS *r* band as a dark (black) long-dashed line, and in the WISE *W1* band as a dark-grey (red) short-dashed line. Each lower panel *Nb* shows the oxygen abundance in individual H II regions as a function of radius. The dark (black) open circles show $(O/H)_{C_{NS}}$ abundances and the grey (red) filled circles indicate the $(O/H)_{T_e}$ abundances. The solid line represents the inferred linear abundance gradient. (A color version of this figure is available in the on-line edition.)

4 DISCUSSION AND CONCLUSIONS

Fig. 2 shows the surface brightness profiles and radial distributions of the oxygen abundances for the irregular galaxies with steep inner profiles. Each galaxy is presented in two panels. Each upper panel *Na* shows the surface brightness profiles in the SDSS *g* band as a light-grey (blue) solid line, in the SDSS *r* band as a dark (black) long-dashed line, and in the WISE *W1* band as a dark-grey (red)

short-dashed line. Each lower panel *Nb* shows the oxygen abundance in individual H II regions (open circles) as a function of radius. The linear best fit to those data is indicated by a solid line. Fig. 2 shows that irregular galaxies with steep inner profiles have appreciable radial abundance gradients.

Fig. 3 shows the surface brightness profiles and radial distributions of the oxygen abundances for irregular galaxies with flat inner profiles. Inspection of Fig. 3 shows that the radial abundance gra-

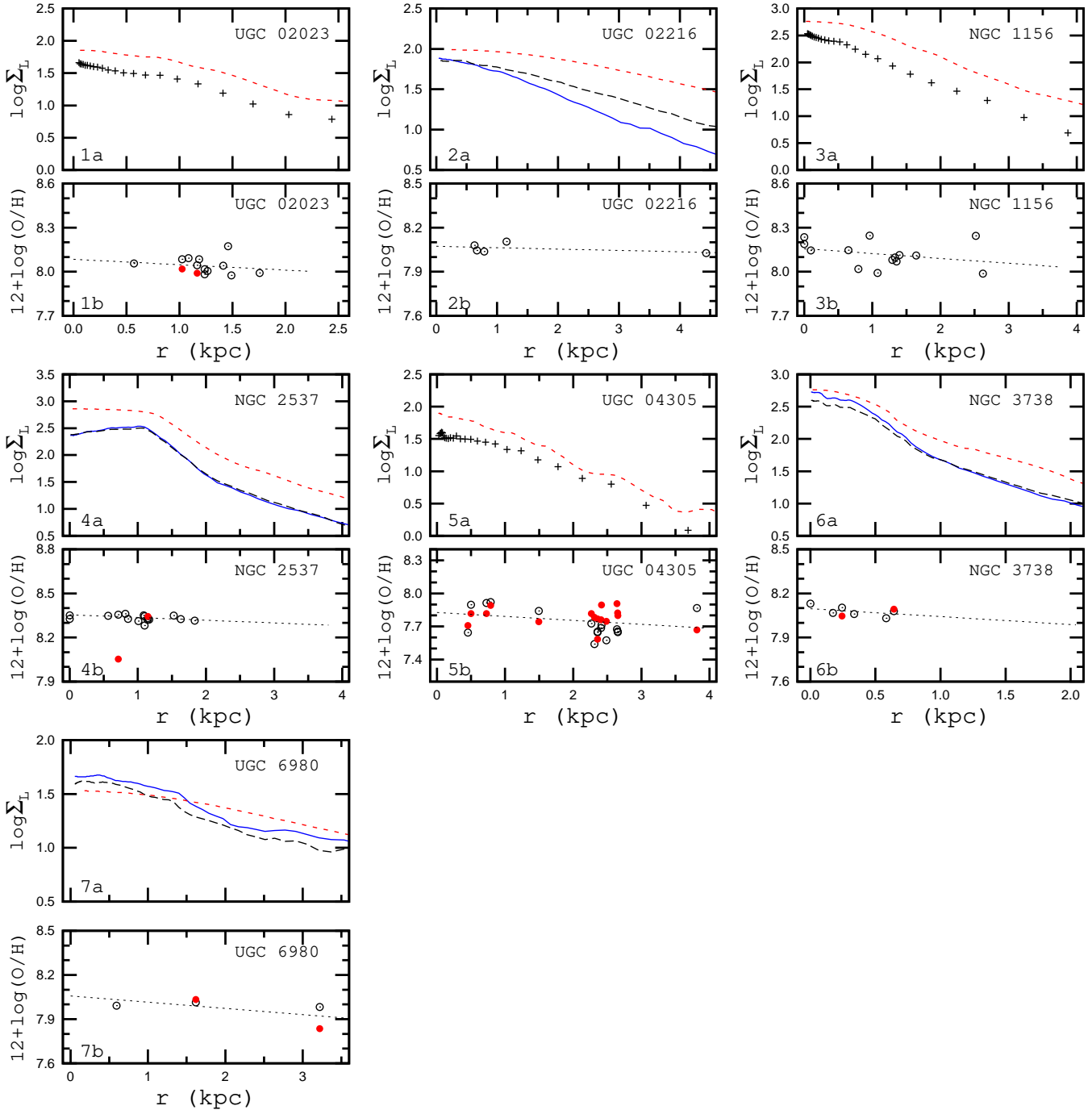


Figure 3. The same as Fig. 2 but for irregular galaxies with flat inner profiles. For galaxies without SDSS photometric maps, the surface brightness profile in the R band from Swaters & Balcells (2002) is indicated with dark (black) plus signs. (A color version of this figure is available in the on-line edition.)

dients in the irregular galaxies with flat inner profiles are shallower than the gradients in irregular galaxies with steep inner profiles.

Thus, our data suggest that there is a relation between the radial abundance gradient in an irregular galaxy and its surface brightness profile. Panel *a* of Fig. 4 shows the radial oxygen abundance gradient as a function of optical radius R_{25} for our sample of irregular galaxies. The dark (black) open circles mark irregular galaxies with steep inner photometric profiles. The dark-grey (red) open squares denote galaxies with flat inner profiles. The dark (black) dotted line is the arithmetic mean of the gradients for galax-

ies with steep inner photometric profiles, whereas the dark-grey (red) dashed line is the mean for galaxies with flat inner photometric profiles. The light-grey (green) solid line is the arithmetic mean of the gradients for all our galaxies (both those with steep and those with flat inner profiles). Since the numbers of galaxies in our samples are small even one deviant galaxy may appreciably change the arithmetic mean for the sample. Indeed the arithmetic mean of the gradients for galaxies with steep inner photometric profiles is changed by ~ 0.05 dex R_{25}^{-1} when the deviating galaxy NGC 4214

Table 2. The derived parameters of the radial oxygen and nitrogen abundance distributions in our target galaxies.

Galaxy	R_{25} kpc	$12+\log(\text{O}/\text{H})_{R_0}$	O/H gradient dex R_{25}^{-1}	$\sigma(\text{O}/\text{H})$ dex	$12+\log(\text{N}/\text{H})_{R_0}$	N/H gradient dex R_{25}^{-1}	$\sigma(\text{N}/\text{H})$ dex	References
UGC 02023	2.24	8.08 ± 0.07	-0.082 ± 0.128 (0.150)	0.052	6.72 ± 0.12	-0.137 ± 0.208 (0.252)	0.085	10, 18
UGC 02216	4.25	8.07 ± 0.02	-0.040 ± 0.043 (0.300)	0.026	6.69 ± 0.05	-0.056 ± 0.091 (0.560)	0.054	16
NGC 1156	3.76	8.16 ± 0.04	-0.124 ± 0.112 (0.138)	0.080	6.84 ± 0.07	-0.232 ± 0.202 (0.260)	0.145	8, 10, 14
NGC 2537	3.80	8.35 ± 0.01	-0.071 ± 0.034 (0.031)	0.014	7.28 ± 0.03	-0.237 ± 0.113 (0.124)	0.046	1, 6, 8, 16
UGC 04305	3.92	7.83 ± 0.04	-0.140 ± 0.078 (0.085)	0.101	6.31 ± 0.05	-0.182 ± 0.090 (0.108)	0.116	3, 4
NGC 3738	2.04	8.10 ± 0.02	-0.110 ± 0.103 (0.128)	0.028	6.71 ± 0.04	-0.144 ± 0.173 (0.201)	0.046	1, 8, 10
UGC 06980	3.55	8.06 ± 0.07	-0.150 ± 0.112 (0.124)	0.056	6.62 ± 0.05	-0.145 ± 0.077 (0.089)	0.038	7, 16
NGC 4214	2.72	8.20 ± 0.05	0.049 ± 0.124 (0.122)	0.090	6.89 ± 0.06	0.037 ± 0.148 (0.189)	0.108	8, 10, 11, 16
NGC 4395	5.47	8.32 ± 0.04	-0.343 ± 0.072 (0.066)	0.064	7.14 ± 0.07	-0.629 ± 0.119 (0.085)	0.104	5, 13, 16, 17
UGC 07557	4.54	8.32 ± 0.06	-0.176 ± 0.118 (0.176)	0.057	7.15 ± 0.14	-0.361 ± 0.280 (0.413)	0.135	15
NGC 4449	3.76	8.26 ± 0.01	-0.207 ± 0.034 (0.063)	0.028	7.03 ± 0.03	-0.369 ± 0.053 (0.122)	0.051	1, 2, 8, 9, 12, 13, 16
CG071-090	1.98	8.19 ± 0.02	-0.344 ± 0.060 (0.074)	0.026	6.86 ± 0.02	-0.525 ± 0.074 (0.104)	0.032	7, 16
UGC 09614	7.23	8.18 ± 0.09	-0.218 ± 0.128 (0.198)	0.063	6.88 ± 0.14	-0.389 ± 0.195 (0.262)	0.096	7, 16
UGC 12709	7.86	8.48 ± 0.08	-0.358 ± 0.113 (0.136)	0.084	7.31 ± 0.15	-0.546 ± 0.210 (0.217)	0.156	16

References: 1 – Berg et al. (2012), 2 – Böker et al. (2001), 3 – Croxall et al. (2009), 4 – Egorov et al. (2013), 5 – Esteban et al. (2009), 6 – Gil de Paz et al. (2000), 7 – Haurberg et al. (1982), 8 – Ho et al. (1997), 9 – Hunter et al. (1982), 10 – Hunter & Hoffman (1999), 11 – Kobulnicky & Skillman (1996), 12 – Lequeux et al. (1979), 13 – McCall et al. (1985), 14 – Moustakas & Kennicutt (2006), 15 – Romanishin et al. (1983), 16 – SDSS (York et al. (2000), 17 – van Zee et al. (1998), 18 – van Zee & Haynes (2006).

(with a positive gradient $0.049 \text{ dex } R_{25}^{-1}$) is excluded from consideration.

Panel *b* of Fig. 4 shows the same as panel *a* but for the nitrogen abundance gradients. Comparison between panels *a* and *b* shows that the general picture is similar for oxygen and nitrogen abundance gradients, i.e., the irregular galaxies with flat inner photometric profiles have shallower nitrogen abundance gradients as compared to galaxies with steep inner photometric profiles.

Panel *c* of Fig. 4 shows the radial oxygen abundance gradients with bootstrapped errors (reported in Table 2 in parenthesis). The filled dark (black) circle on the right side of the panel shows the mean value of the gradients within its 95% and 68% confidence intervals for the sample of galaxies with steep inner photometric profiles. To estimate the confidence interval of the mean value of the gradients of the sample of galaxies the bootstrap method is used. We create 10^5 bootstrapped subsamples from the original sample of gradients keeping the size of each bootstrapped subsample equal to the size of the original sample, and modifying the value of the original gradient of each galaxy by introducing a random error. This error is randomly chosen from a set of errors that follow a Gaussian distribution scaled to the standard deviation corresponding to the bootstrapped error of abundance gradient (reported in Table 2 in parenthesis). We consider the distribution of the mean values of the abundance gradients for those 10^5 bootstrapped subsamples and determine the 95% and 68% confidence intervals of the mean abundance gradient for the sample of galaxies. The filled dark-grey (red) square shows such a mean value of the abundance gradients for the sample of galaxies with flat inner photometric profiles, and the light-grey (green) asterisk shows the one for the total sample of galaxies. Panel *d* of Fig. 4 shows the same as panel *c* but for the radial nitrogen abundance gradients.

The difference between the mean values of the oxygen abundance gradients for galaxies with steep and flat inner photometric profiles is estimated in a similar way and amounts to $-0.126 \text{ dex } R_{25}^{-1}$ within the 95% confidence interval ($-0.306, 0.059$). The difference between the mean values of the nitrogen abundance gradients is $-0.236 \text{ dex } R_{25}^{-1}$ within the 95% confidence interval ($-0.540,$

0.073). The difference between the mean values of the abundance gradients in irregular galaxies with steep and flat inner photometric profiles exists (is less than 0) at 91% confidence level for oxygen abundance gradients and at 94% confidence level for nitrogen abundance gradients.

Thus, our data suggest that *i*) there are radial abundance gradients in irregular galaxies, and *ii*) there is a difference between radial abundance gradients in irregular galaxies with steep and flat inner photometric profiles with a probability higher than 90%.

It should be noted that here the abundances are determined through the *C* and *T_e* methods. The *C* method is based on the abundances derived via the *T_e* method and, consequently, produces the abundances on the same metallicity scale as the *T_e* method. If the abundances derived using the *T_e* method are not correct for some reason (e.g., because of small-scale temperature fluctuations within an H II region (Peimbert 1967), or if the energies of the electrons in an H II region do not follow a Maxwell distribution (Dopita et al. 2013)) then our abundances should be revised. Furthermore, the absolute metallicity scale of H II regions varies up to ~ 0.7 dex depending on the calibration used (Kewley & Ellison 2008). As was noted above, a prominent characteristic of the previous calibrations is that they are not applicable across the whole range of metallicities of H II regions but only within a limited interval. The oxygen abundances of irregular galaxies typically are within or near the transition zone in the $R_{23} - \text{O}/\text{H}$ diagram where previous calibrations cannot be used or where they provide abundances with large uncertainties. Therefore the *T_e*- and *C*-based abundances are preferable for irregular galaxies.

It is known (e.g., Searle & Sargent 1972; Pagel 1997) that the radial distribution of oxygen abundances in the disk of a galaxy is controlled by the variation of the astration level (or gas mass fraction μ) with radius and by the mass exchange between a galaxy and the surrounding medium (via galactic winds and/or gas infall/merging) and between different parts of a galaxy. Taking into consideration the radial variation of the astration level, one may expect that physical gradients (expressed in dex kpc^{-1}) in irregular galaxies can be even steeper than those in spiral galaxies. The

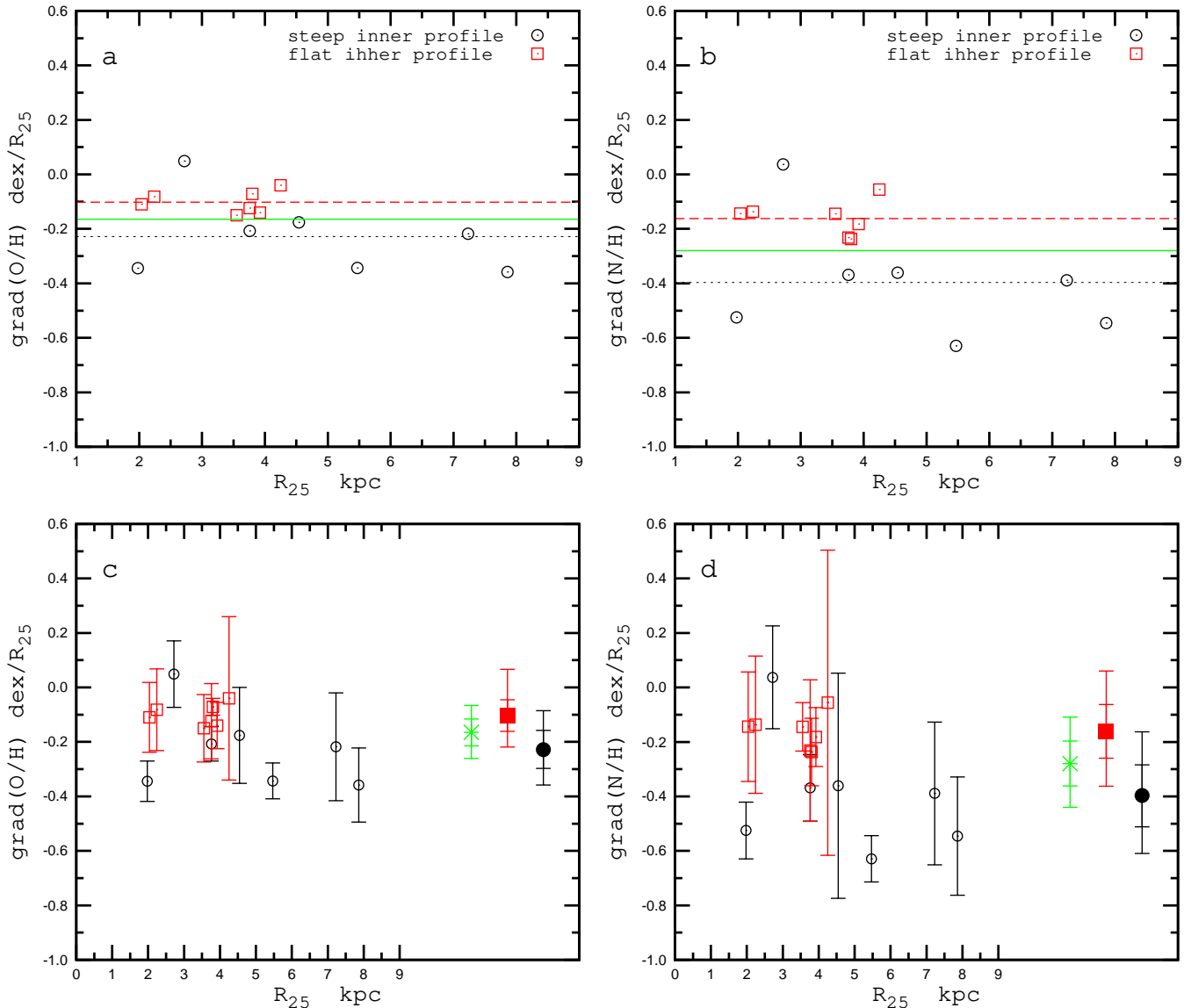


Figure 4. The panel *a* shows the oxygen abundance gradient as a function of optical radius R_{25} . The dark (black) open circles mark irregular galaxies with steep inner photometric profiles. The dark-grey (red) open squares denote galaxies with flat inner photometric profiles. The dark (black) dotted line is the arithmetic mean of the gradients for galaxies with steep inner profiles, the dark-grey (red) dashed line for galaxies with flat inner profiles, and the light-grey (green) solid line the total sample. Panel *b* shows the same as panel *a* but for the nitrogen abundance gradients. Panel *c* shows the oxygen abundance gradients with bootstrapped errors. On the right side of the panel, the mean values of the gradients for the sample of galaxies with steep inner photometric profiles (the filled dark (black) circle), for the sample of galaxies with flat inner photometric profiles (the filled dark-grey (red) square), and for total sample (the light-grey (green) asterisk) and their 95% and 68% confidence intervals are shown. Panel *d* shows the same as panel *c* but for the nitrogen abundance gradients. (A color version of this figure is available in the on-line edition.)

metallicities in irregular galaxies are typically lower than the ones in spiral galaxies since irregular galaxies are less massive and less evolved. The simple model for the chemical evolution of galaxies predicts that the oxygen abundance O/H varies with gas mass fraction μ more strongly at low metallicity. Thus a similar change of μ along the radial direction would result in a larger change of O/H in irregular galaxies than in spiral galaxies.

Radial mixing of gas flattens the abundance gradient in the disk of a galaxy. Radial mixing of gas can be caused by interacting or merging galaxies (e.g., Rupke et al. 2010a,b) and by galactic fountains (galactic winds and subsequent gas infall). The arguments pro and contra galactic wind-dominated evolution of irregular galaxies are discussed in many studies devoted to the chemical

evolution of galaxies (Skillman 1997; Cavián et al. 2013, among many others). A galactic wind can be caused by the injection of energy by multiple, spatially and temporally clustered supernovae in a galaxy undergoing a starburst (De Young & Gallagher 1990; Mac Low & Ferrara 1999). The efficiency of the galactic winds depends on the number of massive stars that are progenitors of supernovae in a star formation event. Lee et al. (2009) found that continuous, steady star formation dominates in the present epoch in dwarf galaxies. Only $\sim 6\%$ of low-mass galaxies experience strong star formation bursts. The fraction of stars formed in starbursts is $\sim 23\%$. However, it is not clear whether a strong star formation burst can occur with equal probability in every galaxy or whether a starburst happens only in a particular subset of galaxies.

Thus, we can interpret our results in the following manner. Irregular galaxies with steep inner profiles do not seem to undergo strong radial mixing of gas at the present epoch and show considerable radial abundance gradients. The radial mixing of gas (through radial flows or galactic fountains) took place in irregular galaxies with flat inner profiles, resulting in shallower (if any) gradients as compared to the galaxies with steep inner profiles. It should be noted that the physical reason for different radial profile types is still a mystery. It is not even clear why there is an exponential drop-off of the brightness profile (Herrmann et al. 2013).

5 SUMMARY

We determined the abundance distributions traced by H II regions and compare their shape with the surface brightness profiles of the disks of fourteen irregular *Sm* and *Im* galaxies (morphological T types of $T = 9$ and $T = 10$). We used the emission line intensities in published spectra of H II regions from different studies to infer the abundances. The oxygen $(\text{O}/\text{H})_{T_e}$ and nitrogen $(\text{N}/\text{H})_{T_e}$ abundances in the H II regions with the detected auroral line $[\text{O III}]\lambda 4363$ were determined using the equations of the classic T_e -method. In the other H II regions, oxygen $(\text{O}/\text{H})_{\text{CNS}}$ and nitrogen $(\text{N}/\text{H})_{\text{CNS}}$ abundances were obtained through the C method. We then quantified the values of the gradients of the radial abundance profiles.

Moreover, we constructed radial surface brightness profiles in the infrared *W1* WISE band and in the SDSS *g* and *r* bands using the publicly available photometric maps. The irregular galaxies of our sample can be divided into two types according to the shapes of their surface brightness profiles: those with steep inner profiles, and those with flat inner profiles.

We find that there is a correspondence between the radial abundance gradient in an irregular galaxy and its surface brightness profile with a probability higher than 90%. Irregular galaxies with steep inner profiles usually show a considerable radial abundance gradient. Irregular galaxies with flat inner surface brightness profiles have shallower gradients (if any) as compared to galaxies with steep inner profiles.

Thus, irregular galaxies with steep inner profiles show usually a pronounced radial abundance gradient that resembles that of spiral galaxies. In that sense, those irregular galaxies seem to extend the Hubble sequence of spiral galaxies. In other words, our data suggest that there is no “spiral versus irregular dichotomy” in terms of radial abundance gradients existing only in spiral galaxies, but not in irregulars. While irregulars have long been believed to be chemically homogeneous, our study shows that given enough measurements of nebular abundances of H II regions across a wide range of galactocentric radii, irregulars may well exhibit radial abundance gradients. This tendency is particularly conspicuous in irregulars with steep surface brightness profiles in their inner regions.

ACKNOWLEDGEMENTS

We are grateful to the referee for his/her constructive comments. L.S.P., E.K.G., and I.A.Z. acknowledge support within the framework of Sonderforschungsbereich (SFB 881) on “The Milky Way System” (especially subproject A5), which is funded by the German Research Foundation (DFG). L.S.P. and I.A.Z. thank the hospitality of the Astronomisches Rechen-Institut at Heidelberg University where part of this investigation was carried out.

This work was partly funded by the subsidy allocated to Kazan Federal University for the state assignment in the sphere of scientific activities (L.S.P.).

We thank R.A. Swaters and M. Balcells for supporting us with the surface brightness profiles of galaxies from their sample in numerical form.

This research made use of Montage, funded by the National Aeronautics and Space Administration’s Earth Science Technology Office, Computational Technologies Project, under Cooperative Agreement Number NCC5-626 between NASA and the California Institute of Technology. The code is maintained by the NASA/IPAC Infrared Science Archive.

Funding for the SDSS and SDSS-II has been provided by the Alfred P. Sloan Foundation, the Participating Institutions, the National Science Foundation, the U.S. Department of Energy, the National Aeronautics and Space Administration, the Japanese Monbukagakusho, the Max Planck Society, and the Higher Education Funding Council for England. The SDSS Web Site is <http://www.sdss.org/>.

REFERENCES

- Ahn C.P. et al., 2012, *ApJS*, 203, 21
 Alloin D., Collin-Souffrin S., Joly M., Vigroux L., 1979, *A&A*, 78, 200
 Berg D.A. et al., 2012, *ApJ*, 754, 98
 Blanton M.R., Roweis S., 2007, *AJ*, 133, 734
 Böker T., van der Marel R.P., Mazuca L., Rix H.-W., Rudnick G., Ho L.C., Shields J.G., 2001, *AJ*, 121, 1473
 Cardelli J.A., Clayton G.C., Mathis J.S., 1989, *ApJ*, 345, 245
 Casagrande L., Ramírez I., Meléndez J., Asplund M., 2012, *ApJ*, 761, 16
 Cavián M., Ascibar Y., Mollá M., Díaz Á.I., 2013, *MNRAS*, 434, 2491
 Cignoni M., Cole A.A., Tosi M., Gallagher J.S., Sabbi E., Anderson J., Grebel E.K., Nota A., 2013, *ApJ*, 775, 83
 Croxall K.V., van Zee L., Lee H., Skillman E.D., Lee J., Côté S., Kennicutt R.C., Miller B.W., 2009, *ApJ*, 705, 723
 de Vaucouleurs G., de Vaucouleurs A., Corvin H.G., Buta R.J., Paturel G., Fouque P., 1991, *Third Reference Catalog of Bright Galaxies*, New York: Springer Verlag (RC3)
 De Young D.S., Gallagher J.S., 1990, *ApJ*, 356, L15
 Dopita M.A., Sutherland R.S., Nicolls D.C., Kewley L.S., Voght F.P.A., 2013, *ApJS*, 208, 10
 Egorov O.A., Lozinskaya T.A., Moiseev A.V., 2013, *MNRAS*, 429, 1450
 Esteban C., Bresolin F., Peimbert M., García-Rojas J., Peimbert A., Mesa-Delgado A., 2009, *ApJ*, 700, 654
 Garnett D.R., 2002, *ApJ*, 581, 1019
 Gil de Paz A., Zamorano J., Gallego J., Domínguez F. de B., 2000, *A&AS*, 145, 377
 Glatt K. et al., 2008, *AJ*, 136, 1703
 Gusev A.S., Pilyugin L.S., Sakhibov F., Dodonov S.N., Ezhkova O.V., Khramtsova M.S., 2012, *MNRAS*, 424, 1930
 Haurberg N.C., Rosenberg J., Salzer J.J., 2013, *ApJ*, 765, 66
 Herrmann K.A., Hunter D.A., Elmegreen B.G., 2013, *AJ*, 146, 104
 Ho L.C., Filippenko A.V., Sargent W.L.W., 1997, *ApJS*, 112, 315
 Hunter D.A., Hoffman L., 1999, *AJ*, 117, 2789
 Hunter D.A., Gallagher J.S., Rautenkranz D., 1982, *ApJS*, 49, 53
 Karachentsev I.D., Makarov D.I., Kaisina E.I., 2013, *AJ*, 145, 10

- Kewley L.J., Ellison S.L., 2008, *ApJ*, 681, 1183
- Kniazev A.Y., Grebel E.K., Pustilnik S.A., Pramskij A.G., Zucker D.B., 2005, *AJ*, 130, 1558
- Kobulnicky H.A., Skillman E.D., 1996, *ApJ*, 471, 211
- Lee H., Zucker D.B., Grebel E.K., 2007, *MNRAS*, 376, 820
- Lee J.C., Kennicutt R.C., Funes J.G., Sakai S., Akiyama S., 2009, *ApJ*, 692, 1305
- Lequeux J., Peimbert M., Rayo J.F., Serrano A., Torres-Peimbert S., 1979, *A&A*, 80, 155
- Mac Low M.-M., Ferrara A., 1999, *ApJ*, 219, 46
- McCall M.L., Rybski P.M., Shields G.A., 1985, *ApJS*, 57, 1
- Miller B.M., Hodge P., 1996, *ApJ*, 458, 467
- Moustakas J., Kennicutt R.C., 2006, *ApJS*, 164, 81
- Moustakas J., Kennicutt R.C., Tremonti C.A., Dale D.A., Smith J.-D.T., Calzetti D., 2010, *ApJS*, 190, 233
- Pagal B.E.J. 1997, *Nucleosynthesis and Chemical Evolution of Galaxies* (Cambridge: Cambridge Univ. Press)
- Pagal B.E.J., Edmunds M.G., Fosbury R.A.E., Webster B.L., 1978, *MNRAS*, 184, 569
- Pagal B.E.J., Edmunds M.G., Blackwell D.E., Chun M.S., Smith G., 1979, *MNRAS*, 189, 95
- Peimbert M., 1967, *ApJ*, 150, 825
- Pilyugin L.S., Ferrini F., 2000, *A&A*, 358, 72
- Pilyugin L.S., Vílchez J.M., Contini T., 2004, *A&A*, 425, 849
- Pilyugin L.S., Thuan T.X., Vílchez J.M., 2007, *MNRAS*, 376, 353
- Pilyugin L.S., Vílchez J.M., Thuan T.X., 2010, *ApJ*, 720, 1738
- Pilyugin L.S., Grebel E.K., Mattsson L., 2012, *MNRAS*, 424, 2316
- Pilyugin L.S., Lara-López M.A., Grebel E.K., Kehrig C., Zinchenko I.A., López-Sánchez Á.R., Vílchez J.M., Mattsson L., 2013, *MNRAS*, 432, 1217
- Pilyugin L.S., Grebel E.K., Kniazev A.Y., 2014a, *AJ*, 147, 131
- Pilyugin L.S., Grebel E.K., Zinchenko I.A., Kniazev A.Y., 2014b, *AJ*, 148, 134
- Romanishin W., Strom K.M., Strom S.E., 1983, *ApJS*, 53, 105
- Roy J.-R., Belley J., Dutil Y., Martin P., 1996, *ApJ*, 460, 284
- Rupke D.S.N., Kewley L.J., Barnes J.E., 2010, *ApJ*, 710, L156
- Rupke D.S.N., Kewley L.J., Chien L.-H., 2010, *ApJ*, 723, 1255
- Sánchez S.F. et al., 2014, *A&A*, 563, 49
- Schlafly E.F., Finkbeiner D.P., 2011, *ApJ*, 737, 103
- Schlegel D.J., Finkbeiner D.P., Davis M., 1998, *ApJ*, 500, 525
- Searle L., Sargent W.L.W., 1972, *ApJ*, 173, 25
- Skillman E.D., 1997, *RevMexAA (Serie de Conferencias)*, 6, 36
- Swaters R.A., Balcells M., 2002, *A&A*, 390, 863
- Taylor V.A., Jansen R.A., Windhorst R.A., Odewahn S.C., Hibbard J.E., 2005, *ApJ*, 630, 784
- van Zee L., Haynes M.P., 2006, *ApJ*, 636, 214
- van Zee L., Salzer J.J., Haynes M.P., O'Donoghue A. A., Balonek T.J., 1998, *AJ*, 116, 2805
- Vila-Costas M.B., Edmunds M.G. 1992, *MNRAS*, 259, 121
- Wright E.L. et al., 2010, *AJ*, 140, 1868
- York D.G. et al., 2000, *AJ*, 120, 1579
- Zaritsky D., Kennicutt R.C., Huchra, J.P., 1994, *ApJ*, 420, 87